Cement and Concrete Research 40 (2010) 460–472

Contents lists available at ScienceDirect

Cement and Concrete Research

journal homepage: http://ees.elsevier.com/CEMCON/default.asp

A micromechanical approach to elastic and viscoelastic properties of fiber reinforced concrete

V.F. Pasa Dutra, S. Maghous *, A. Campos Filho, A.R. Pacheco

[a] Department of Civil Engineering, Federal University of Rio Grande do Sul, Porto Alegre, RS, Brazil

ARTICLE INFO

Article history:
Received 9 June 2009
Accepted 21 October 2009

Keywords:
Short-fiber composite
Creep (C)
Micromechanics (C)

ABSTRACT

Some aspects of the constitutive behavior of fiber reinforced concrete (FRC) are investigated within a micromechanical framework. Special emphasis is put on the prediction of creep of such materials. The linear elastic behavior is first examined by implementation of a Mori–Tanaka homogenization scheme. The micromechanical predictions for the overall stiffness prove to be very close to finite element solutions obtained from the numerical analysis of a representative elementary volume of FRC modeled as a randomly heterogeneous medium.

The validation of the micromechanical concepts based on comparison with a set of experiments, shows remarkable predictive capabilities of the micromechanical representation.

The second part of the paper is devoted to non-ageing viscoelasticity of FRC. Adopting a Zener model for the behavior of the concrete matrix and making use of the correspondence principle, the homogenized relaxation moduli are derived analytically. The validity of the model is established by mean of comparison with available experiment measurements of creep strain of steel fiber reinforced concrete under compressive load. Finally, the model predictions are compared to those derived from analytical models formulated within a one-dimensional setting.

1. Introduction

Assessment of the macroscopic properties of composite materials is one of the major concerns in material and structural engineering. As far as the elastic properties of composites are concerned, the micromechanical techniques are nowadays widely applied and have proves successful. This is particularly the case for composites with periodic microstructure.

Nevertheless, the application of micromechanical tools to the modeling of non-linear behavior of composites, and more specifically for composites with randomly distributed phases, is relatively recent and several issues are still open [1]. In particular, the determination of viscoelastic or strength properties of randomly heterogeneous material remains an important task.

In this context, fiber reinforced concrete (FRC) represents a typical example of disordered material. FRC is a cement-based composite with improved mechanical properties in terms of tensile strength or fracture toughness. Such a material results from the association of a cement matrix and embedded fibers. Fibers used in the reinforcement of the concrete generally fall within one of the following four categories [2]: natural (sisal, coconut, bamboo, and jute), synthetic (acrylic, aramid, carbon, nylon, polyester, polyethylene, and polypropylene), glass and steel fiber. The main role of fiber addition is to minimize the emergence and propagation of cracks [3]. In addition, steel fibers are increasingly used as full or partial replacement of conventional web reinforcement in some structural concrete applications [4–6], since their inclusion in concrete mix has been shown to enhance shear resistance and ductility.

Owing to the well-established performance of FRC, major efforts have been dedicated during the last decade to the modeling of its behavior. A traditional way to formulate the behavior of FRC is the phenomenological approach which consists in identifying the constitutive laws by means of laboratory tests [7–9]. The advantage of this approach lies on the direct access to material information at the relevant scale for the analysis of the structure. On the other hand, the main limitation of such phenomenological reasoning is connected with the extensive and costly experimental programs, which a complete characterization of the constitutive behavior would require.

An attractive alternative to handling this kind of problem is provided by the framework of micromechanics. The scale adopted for the description of the composite components (i.e., phase properties and morphological information) is referred to as the microscopic scale, while the macroscopic scale is the engineer scale, i.e., that is considered for the analysis of the structure response under prescribed loading. Taking advantage of the condition of scale separation [1], FRC can therefore be regarded from a macroscopic viewpoint as a homogenized medium. Implementing the homogenization techniques (see for instance, [10–15]), the properties of the latter are evaluated from those of its constituents as well as from the knowledge of the shape and volume fraction of fibers.

* Corresponding author. Tel.: +55 51 33 08 35 88; fax: +55 51 33 08 39 99.
E-mail address: samir.maghous@ufrgs.br (S. Maghous).

0008-8846/$ – see front matter © 2009 Elsevier Ltd. All rights reserved.
doi:10.1016/j.cemconres.2009.10.018

In the case of disordered materials such FRC, the basic approach of the micromechanical approach is to consider the traditional representative elementary volume (REV) as a heterogeneous structure. Its response to a mechanical loading is then analyzed in the framework of a boundary value problem [16]. The effective behavior of the composite is obtained from the solution to this boundary value problem.

The purpose of the present paper is to investigate in the context of homogenization, some aspects related to elastic and viscoelastic behaviors of FRC. The ideas developed herein assume a matrix/inclusion morphology for FRC. The fibers are modeled as flat prolate spheroids, and a Mori–Tanaka homogenization scheme [17–19] is then used to obtain estimates for the overall elastic properties.

This paper is organized as follows. Section 2 deals with the elastic behavior of FRC. After a brief recall of the principle of elastic homogenization, estimates of the effective elastic properties are derived. The accuracy of the analytical approach is assessed by comparison with finite element solutions as well as with available experimental results. Section 3 is devoted to the formulation of the non-ageing viscoelastic behavior of FRC. Invoking the principle of elastic–viscoelastic correspondence, the approach takes advantage of the results previously obtained in elasticity.

Notations: throughout the paper, the following notations are adopted

a	scalar;
$\underline{a}$	vector;
$\underline{\underline{a}}$	second-order tensor;
$\underline{\underline{\underline{\underline{a}}}}$	fourth-order tensor.

In addition, small characters refer to microscopic quantities, whereas capital characters refer to macroscopic quantities. For instance, $\underline{\sigma}$ and $\underline{\underline{\Sigma}}$ denote respectively the microscopic and macroscopic stress tensors.

2. Macroscopic properties of fiber reinforced concrete

This section deals with the evaluation of the elastic properties of FRC. First, a very brief introduction to micromechanics and homogenization in linear elasticity is provided. The approach is then applied in Subsection 2.3 to the specific case of FRC by the implementation of a Mori–Tanaka homogenization scheme.

2.1. Principle of elastic homogenization

The homogenization approach basically aims at estimating the effective behavior of a composite material. The main interest of the approach lies on the possibility to use the obtained effective behavior to perform computations at the scale of the structure, considering the homogenized structure instead of the initial heterogeneous one (Fig. 1). A central concept of the homogenization procedure is the existence of a representative elementary volume (REV) of characteristic size l which must comply with the two conditions:

- l is small enough compared to the characteristic size L of the structure, expressing that the RVE is an infinitesimal (elementary) part of the structure;
- l is large enough compared to the dimension d of heterogeneities within the REV, expressing that the latter contains a sufficient number of heterogeneities to be representative of the heterogeneous medium.

The conjunction of the above restrictions is referred to as the scale separation condition $d \ll l \ll L$. It expresses in mathematical terms a necessary condition for the validity of the REV concept.

In the case of a FRC having fibers with a characteristic length of few centimeters $d \sim$ cm, the size of the REV should be of the order of magnitude of few decimeters $l \sim$ cm, and the dimension of the structural element must be at least of few meters $L \sim$ m.

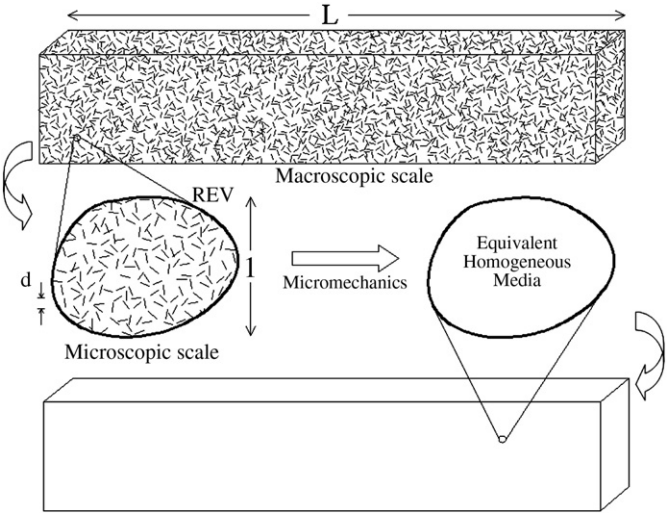

Fig. 1. Schematic description of the homogenization process.

Once the geometry of the REV is completely defined (volume V of the REV and its boundary ∂V), the micromechanical point of view consists of defining a mechanical boundary value problem on the whole REV by imposing homogeneous strain boundary conditions. This is achieved by means of a prescribed displacement $\underline{u}$ along the boundary ∂V of the REV (Fig. 2):

$$\underline{u}(\underline{x}) = \underline{\underline{E}} \cdot \underline{x} \quad \forall \underline{x} \in \partial V \tag{1}$$

where the given strain tensor $\underline{\underline{E}}$ represents in fact the macroscopic strain since it can readily be shown that

$$\langle \underline{\underline{\varepsilon}} \rangle = \frac{1}{V}\int_V \underline{\underline{\varepsilon}}(\underline{x})dV = \frac{1}{2V}\int_{\partial V}(\underline{u}\otimes\underline{n} + \underline{n}\otimes\underline{u})dS = \underline{\underline{E}} \tag{2}$$

$\underline{n}$ denoting the outer normal to ∂V. The above relation indicates that $\underline{\underline{E}}$ is the volume average of the macroscopic strain field $\underline{\underline{\varepsilon}}$ over the whole REV.

On the other hand, the macroscopic stress tensor is taken by definition as the volume average over the whole REV of the local (microscopic) stress field $\underline{\sigma}$:

$$\underline{\underline{\Sigma}} = \langle \underline{\sigma} \rangle = \frac{1}{V}\int_V \underline{\sigma}(\underline{x})dV \tag{3}$$

In the framework of linear elastic homogenization of random heterogeneous material, the macroscopic constitutive equation reads

$$\underline{\underline{\Sigma}} = \underline{\underline{\underline{\underline{C}}}}^{\text{hom}} : \underline{\underline{E}} \tag{4}$$

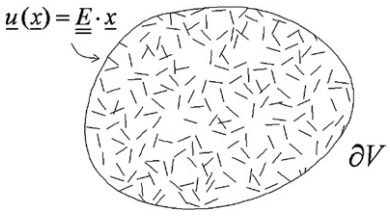

Fig. 2. Loading of the REV: uniform strain boundary conditions.

where $\underset{\sim}{C}^{\hom}$ denotes the overall homogenized (macroscopic) elasticity tensor

$$\underset{\sim}{C}^{\hom} = \sum_{r=1}^{n} f_r \, \underset{\sim}{c}^r : \langle \underset{\sim}{A} \rangle_r \tag{5}$$

in which n is the number of different phases of the REV, f_r the volume fraction of phase r and $\underset{\sim}{c}^r$ the stiffness tensor of phase r. The fourth-order tensor $\underset{\sim}{A}$ is the so-called strain concentration tensor and $\langle \underset{\sim}{A} \rangle_r$ is the corresponding volume average over the domain occupied by phase r:

$$\langle \underset{\sim}{A} \rangle_r = \frac{1}{V_r} \int_{V_r} \underset{\sim}{A}(\underline{x}) dV. \tag{6}$$

It should be recalled that the concentration tensor establishes the link between the macroscopic strain and the local strain at point $\underline{x}$ of the REV: $\underline{\varepsilon}(\underline{x}) = \underset{\sim}{A}(\underline{x}) : \underline{E}$.

The one-step homogenization approach described above falls within the general category of hierarchical multiscale homogenization modeling. In continuum micromechanics, hierarchical vision of the microstructure involves computing information at smaller scales and moving towards the top of the simulation ladder by coursing degrees of freedom as one goes from finer to coarser scales. If a single phase itself exhibits a heterogeneous microstructure, its mechanical behavior can be estimated by introduction of REVs within this phase of much smaller dimensions, leading to a multi-step homogenization scheme, as it has been done for the prediction of macroscopic elastic properties of cement-based materials [20,21].

As far as the numerical evaluation of the overall response of a heterogeneous structure is concerned (and not the explicit assessment of the homogenized material properties), the variational multiscale method [22] provides a computational paradigm for handling of hierarchical multiscale homogenization procedures in solid mechanics, allowing to address applications where the assumption of scale separation as the basis for homogenization methods in continuum micromechanics does not hold (see for instance [23–25]).

2.2. Estimate schemes in linear elastic homogenization

As emphasized by Eq. (5), the determination of the overall elasticity tensor requires being able to compute estimates of the average of strain concentration tensor over each phase r. This is usually achieved through an appropriate homogenization scheme integrating some information on the microstructure morphology.

First, the fibers are randomly distributed within concrete. They are represented by a set of flat prolate spheroids which differ in orientation. For simplicity, an isotropic orientation distribution is assumed. The spherical coordinates (r,θ,φ) and the associated base $(\underline{e}_r, \underline{e}_\theta, \underline{e}_\varphi)$ are used as shown in Fig. 3. Each orientation (θ,ϕ) of the space defines a phase, i.e., the family of solid prolate spheroids whose major axis direction is parallel to $\underline{e}_r$.

Second, the average strain concentration tensor $\langle \underset{\sim}{A} \rangle_r$ is estimated by the Eshelby inhomogeneity problem [26]. From the viewpoint of Eshelby-based theory, the average strain concentration tensor $\langle \underset{\sim}{A} \rangle_r$ is estimated from the uniform strain which establishes in an ellipsoidal inhomogeneity with stiffness $\underset{\sim}{c}^r$ embedded in an infinite medium (reference medium) with stiffness $\underset{\sim}{c}^0$ and subjected to uniform strains at infinity. The corresponding estimate reads

$$\langle \underset{\sim}{A} \rangle_r^{\text{est}} = \left[\underset{\sim}{1} + \underset{\sim}{P}^{0,r} : \left(\underset{\sim}{c}^r - \underset{\sim}{c}^0 \right) \right]^{-1} : \left\langle \left[\underset{\sim}{1} + \underset{\sim}{P}^0 : \left(\underset{\sim}{c} - \underset{\sim}{c}^0 \right) \right]^{-1} \right\rangle^{-1}. \tag{7}$$

In Eq. (7), $\underset{\sim}{P}^{0,r}$ is the fourth-order Hill tensor characterizing the interaction between the inclusion (subscript r) and the reference matrix (subscript 0). $\underset{\sim}{P}^{0,r}$ depends on the stiffness properties $\underset{\sim}{c}^0$ of the reference matrix, as well as on the shape and the orientation (θ,ϕ) of the inclusion. As regards the shape of each fiber, it is defined by the aspect ratio $\alpha = a/b$ of the representing prolate spheroid (Fig. 3). Note that scalars a and b refer respectively to the equatorial radius (semi-major axis) and to the polar radius (semi-minor axis). Accordingly, $\underset{\sim}{P}^{0,r} = \underset{\sim}{P}^{0,r}(\theta,\varphi,\alpha)$.

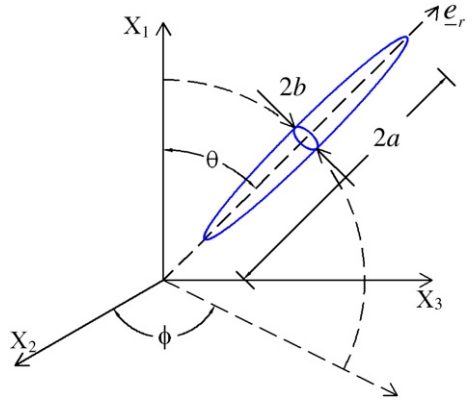

Fig. 3. Geometrical description of the fiber in local spherical coordinates.

Closed-form analytical expressions of Hill tensor $\underset{\sim}{P}^{0,r}$, or equivalently of the so-called Eshelby tensor $\underset{\sim}{S}^{0,r} = \underset{\sim}{P}^{0,r} : \underset{\sim}{c}$, are available for particular configurations of material symmetry and inclusion shape. At this purpose, one may refer for instance to [27–30], to cite a few.

Substitution of Eq. (7) into Eq. (5) yields the sought estimate for the homogenized (macroscopic) elasticity tensor

$$\underset{\sim}{C}^{\hom,\text{est}} = \left\langle \underset{\sim}{c} : \left[\underset{\sim}{1} + \underset{\sim}{P} : \left(\underset{\sim}{c} - \underset{\sim}{c}^0 \right) \right]^{-1} \right\rangle : \left\langle \left[\underset{\sim}{1} + \underset{\sim}{P}^0 : \left(\underset{\sim}{c} - \underset{\sim}{c}^0 \right) \right]^{-1} \right\rangle^{-1}. \tag{8}$$

Clearly enough, the shape of the ellipsoid adopted in the Eshelby inhomogeneity problem for representing a given phase, as well as the choice of the reference medium stiffness $\underset{\sim}{c}^0$ both depend on the morphology of the microstructure. For example, in the self-consistent scheme [31,32], each phase is modeled in the Eshelby inhomogeneity problem as an ellipsoid embedded into the sought homogenized material: $\underset{\sim}{c}^0 = \underset{\sim}{C}^{\hom}$. This kind of scheme is classically used to model perfectly disordered materials such as polycrystal-like microstructures. When a matrix phase m surrounding all the others can be clearly identified, the Mori–Tanaka scheme [17,18] adopts this matrix as the reference medium in the Eshelby inhomogeneity problem: $\underset{\sim}{c}^0 = \underset{\sim}{c}^m$.

2.3. Elastic properties of FRC

In the present work, FRC is modeled as a homogenous concrete matrix with isotropically distributed embedded fibers. Let us first comment on the assumption related to the homogeneity of the concrete matrix. This homogeneity means that the scale of the REV (microscopic scale) is such that the fibers are the only heterogeneities considered for FRC. This implicitly means that such homogeneity results from a previous homogenization process that had been performed in order to take into account the possible micro-cracks present at a smaller scale than the microscopic one. This procedure obviously assumes that the characteristic size of the micro-cracks is smaller enough when compared to that of fibers. Hence, the behavior considered for the concrete matrix, characterized in the present analysis by the corresponding elasticity tensor $\underset{\sim}{c}^0 = \underset{\sim}{c}^m$ results from such a preliminary homogenization. Numerous works have been dedicated to the latter process in order to model the effect of micro-

cracks on the overall elastic properties of a material. For this purpose, one may refer for instance to [12,33–37], to cite a few.

Owing to the matrix–inclusion morphology of FRC, the Mori–Tanaka scheme can be used to estimate the homogenized stiffness tensor. Accordingly, Eq. (8) writes for a uniform orientation distribution of fibers

$$\underset{\sim}{C}^{\hom,\mathrm{MT}} = \left\{(1-f)\,\underset{\sim}{c}^{m} + f\,\underset{\sim}{c}^{f} : \left\langle\left[\underset{\sim}{1} + \underset{\sim}{P}^{m,\alpha} : \left(\underset{\sim}{c}^{f} - \underset{\sim}{c}^{m}\right)\right]^{-1}\right\rangle_{\text{fibers}}\right\} : \left\{(1-f)\,\underset{\sim}{1} + f\left\langle\left[\underset{\sim}{1} + \underset{\sim}{P}^{m,\alpha} : \left(\underset{\sim}{c}^{f} - \underset{\sim}{c}^{m}\right)\right]^{-1}\right\rangle_{\text{fibers}}\right\}^{-1} \quad (9)$$

with

$$\left\langle\left[1 + P^{m,\alpha} : \left(c^{f} - c^{m}\right)\right]^{-1}\right\rangle_{\text{fibers}} = \int_{\varphi=0}^{2\pi}\int_{\theta=0}^{\pi}\left[\underset{\sim}{1} + \underset{\sim}{P}^{m,\alpha}(\theta,\phi) : \left(\underset{\sim}{c}^{f} - \underset{\sim}{c}^{m}\right)\right]^{-1}\frac{\sin\theta}{4\pi}\,d\theta d\phi \quad (10)$$

where f denotes the volume fractions of fibers, $\underset{\sim}{c}^{f}$ the stiffness tensor of fibers and $\underset{\sim}{P}^{m,\alpha}$ is the Hill tensor for prolate spheroid with aspect ratio α.

Assumption of elastic isotropy for both concrete matrix and fibers implies the elastic isotropy of FRC at the macroscopic level. The homogenized elasticity tensor $\underset{\sim}{C}^{\hom,\mathrm{MT}}$ can therefore be completely defined by means of the homogenized bulk modulus $K^{\hom}$ and shear modulus $G^{\hom}$. These coefficients depend on the elastic modulus of concrete matrix (k^m,g^m) and fibers (k^f,g^f), as well on the volume fraction f and aspect ratio α of fibers. The analytical expressions of $K^{\hom}$ and $G^{\hom}$ are obtained from Eqs. (9) and (10) through the evaluation of double integral terms, which can be achieved making use of a formal software, such as the MAPLE software. These expressions are provided in the Appendix for the particular case $\alpha = a/b \to +\infty$, that is the case where the diameter parallel to the axis of revolution is considerably larger than the diameter perpendicular to the axis of revolution.

The effect of the aspect ratio of steel fibers on elasticity of FRC has been extensively investigated [7–9]. It has been found, that for volume fractions of fiber ranging within usual values ($f \leq 5\%$), the aspect ratio of fibers have a small influence on the elastic properties of the steel fiber reinforced concrete. Considering several values for the aspect ratio $\alpha \in \{10, 40, 80, 100, +\infty\}$, a parametric study has been carried (for sake of shortness, this study is not developed here). The micromechanical model predictions in terms of $K^{\hom}$ and $G^{\hom}$ confirmed that the value of α very slightly affects these moduli. In particular, as far as the elastic properties of steel reinforced concrete are concerned, one may reasonably consider an infinite value for α.

An important aspect of the behavior of FRC is related to the impact of fibers' nature on the overall properties. Table 1 shows the elastic properties of some typical fibers.

The influence of elastic properties of the reinforcing fibers is quite notable as emphasized by the results displayed in Figs. 4 and 5.

Table 1
Elastic properties of concrete matrix and different types of fibers.

Fiber	Poisson ratio ν	Young modulus E (MPa)	Bulk modulus k (MPa)	Shear modulus g (MPa)
Steel	0.30	210,000	175,000	80,769.23
Aramid	0.35	62,000	68,888.9	22,963
Carbon	0.20	380,000	211,111.1	158,333.3
Polypropylene	0.30	4000	3333.3	1538.5
Glass AR	0.22	80,000	47,619	32786.9
Concrete	0.20	31,000	17,222.2	12,916.7

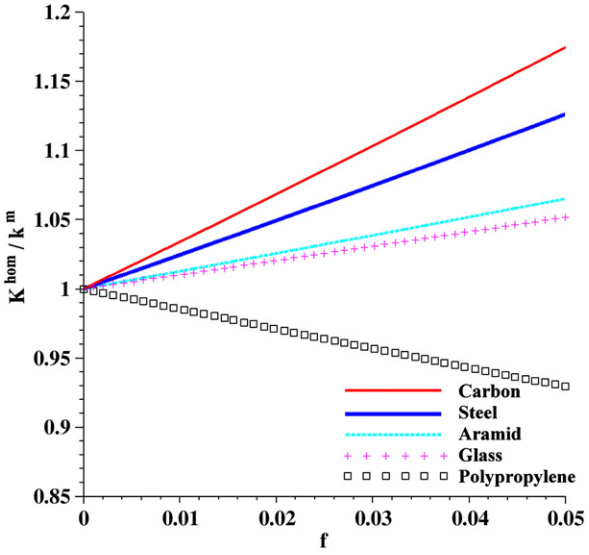

Fig. 4. Influence of reinforcing fiber type on the homogenized bulk modulus of FRC.

2.4. Comparison with experimental results

The micromechanical predictions of FRC elastic properties using a results Mori–Tanaka scheme are compared herein to available experimental results performed on steel fiber reinforced concrete. The values of Young modulus and Poisson ratio of the composite components as provided in the experimental studies are listed in Table 2.

In Thomas and Ramaswamy's [8] experiments, the aspect ratio of the used steel fibers was $\alpha = 55$ and several volume fractions were tested $f \in \{0.5\%, 1\%, 1.5\%\}$. Figs. 6 and 7 respectively display the Mori–Tanaka estimates of $E^{\hom}$ and $\nu^{\hom}$, together with the experimental results.

The Ashour et al. experiments [7] correspond to steel fibers with steel fibers with an aspect ratio of $\alpha = 75$ and $f \in \{0.5\%, 1\%\}$, while $\alpha = 100$ and $f \in \{1\%, 1.5\%, 2.5\%\}$ in the tests performed by Williamson [38]. The comparison of the micromechanical estimates of the homogenized Young modulus with the experimental results are shown in Figs. 8 and 9.

As it appears from the above figures, the Mori–Tanaka estimates prove to be slightly lower than the measured values provided in the mentioned experimental works [7,8,38]. A good agreement is obtained and the consistency with experimental data can be termed as reasonable. The discrepancy observed between the micromechanical predictions of $E^{\hom}$ and the experimental results remains lower than 10%.

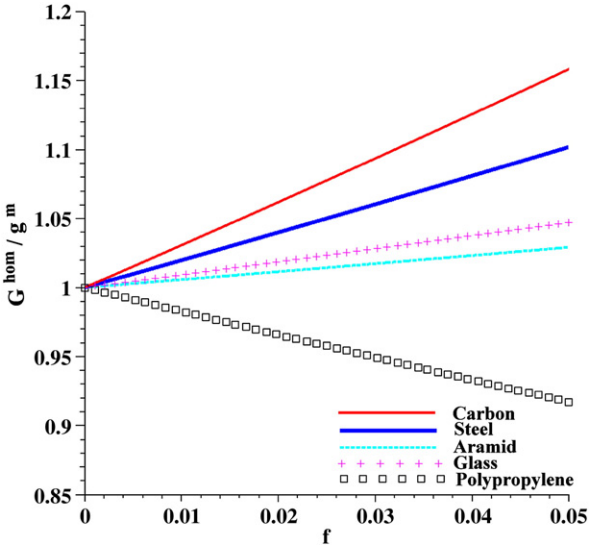

Fig. 5. Influence of reinforcing fiber type on the homogenized shear modulus of FRC.

Table 2
Material properties of steel fiber and concrete.

Fiber	Young modulus E (MPa)	Poisson ratio (ν)
Thomas and Ramaswamy [8]		
Steel fiber	210,000	0.300
Concrete 35 MPa C35	28,700	0.182
Concrete 65 MPa C65	37,500	0.201
Concrete 85 MPa C85	41,700	0.210
Ashour et al. [7]		
Steel fiber	210,000	0.300
Normal Strength Concrete NSC	24,612	0.200
Medium Strength Concrete MSC	35,443	0.200
High Strength Concrete HSC	38,423	0.200
Williamson [38]		
Steel fiber	200,000	0.300
Concrete	20,802	0.2081

2.5. Finite element numerical simulations

In order to assess the accuracy of the Mori–Tanaka estimates, the concentration problem (Eq. (4)) is now solved numerically through the implementation of a finite element (FE) method.

For sake of simplicity, a cubic REV of side l is considered. Owing to the macroscopic isotropy of FRC, the restriction of the analysis to a loading mode defined by uniaxial compression is sufficient to obtain the overall elastic properties. Hence, a macroscopic stress $\underline{\underline{\Sigma}} = -\Sigma_l \underline{e}_1 \otimes \underline{e}_1$ with $\Sigma_l \geq 0$ is applied to the REV (Fig. 10). It is recalled that the scale separation condition ensures the equivalence between homogeneous boundary strain and stress conditions on the REV [39]. Owing to the symmetry conditions, only an eighth of the REV geometry, with appropriate boundary conditions as shown in Fig. 10, is considered for the numerical analysis.

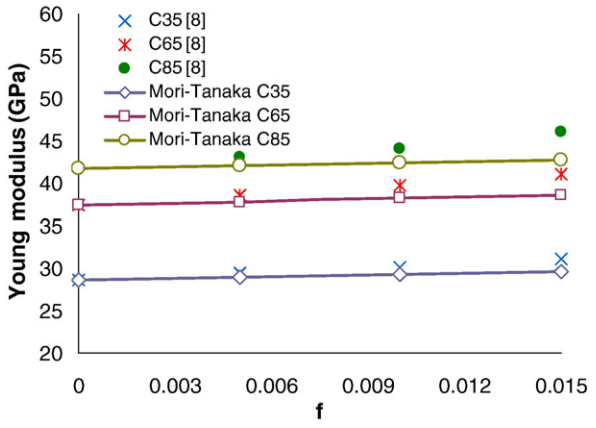

Fig. 6. Young modulus estimated by a Mori–Tanaka scheme and experimentally measured from [8].

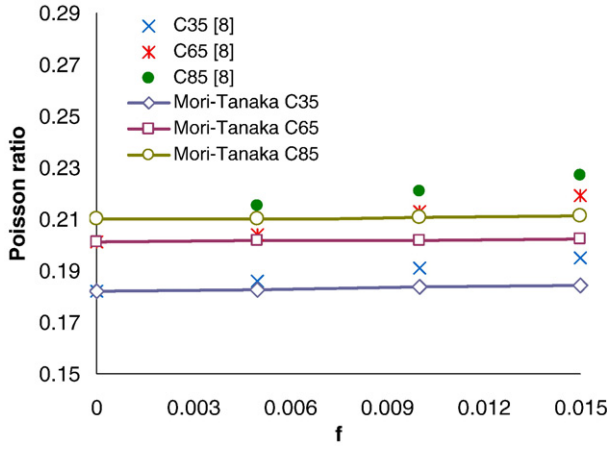

Fig. 7. Poisson ratio estimated by a Mori–Tanaka scheme and experimentally measured from [8].

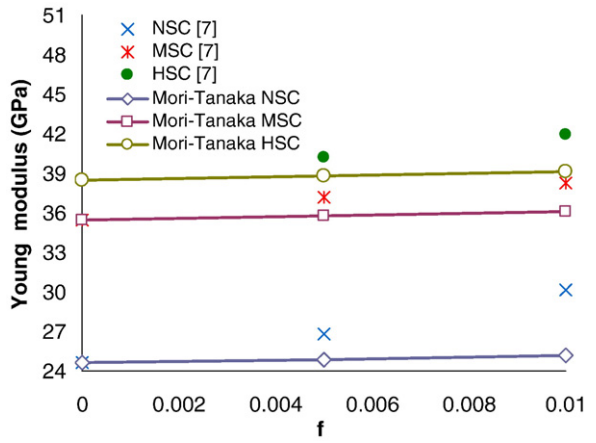

Fig. 8. Young modulus: Mori–Tanaka estimate and experimentally measured value [7].

Twenty nodded quadratic hexahedral elements were used for the concrete discretization of the concrete matrix geometry.

As regards the reinforcement components, the fibers are randomly generated and embedded within the concrete matrix finite elements. It is recalled that perfect bonding is assumed between fibers and concrete matrix. We herein refer to the so-called "embedded model" [40] in which each fiber has the same kinematics than the coincident points of the embedding concrete matrix finite element. Actually, the contribution of the fiber is expressed by an additional term increasing the stiffness of the embedding element. In other terms, the fibers act in the "embedded model" as stiffener elements for the medium.

The spatial distribution and orientation of fibers are randomly generated by means of a specific procedure using the intrinsic function RAN of Fortran programming language.

Once the finite element displacement solution is obtained, the macroscopic strain is computed by means of surface integrals as indicated in Eq. (2). It is expected that

$$\underline{\underline{E}} = -E_l \underline{e}_1 \otimes \underline{e}_1 + E_t(\underline{e}_2 \otimes \underline{e}_2 + \underline{e}_3 \otimes \underline{e}_3) \quad \text{with} \quad E_l, E_t \geq 0. \tag{11}$$

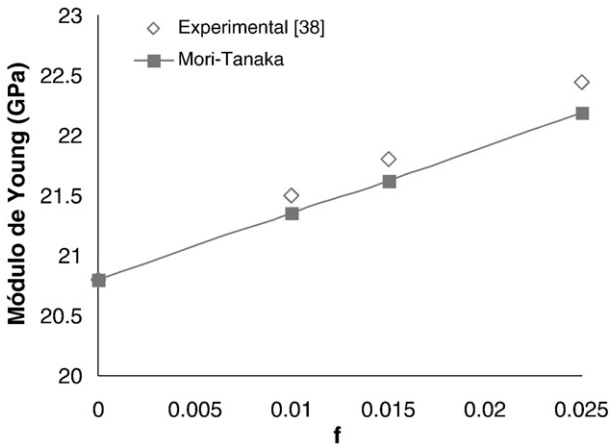

Fig. 9. Young modulus: Mori–Tanaka estimate and experimental data [38].

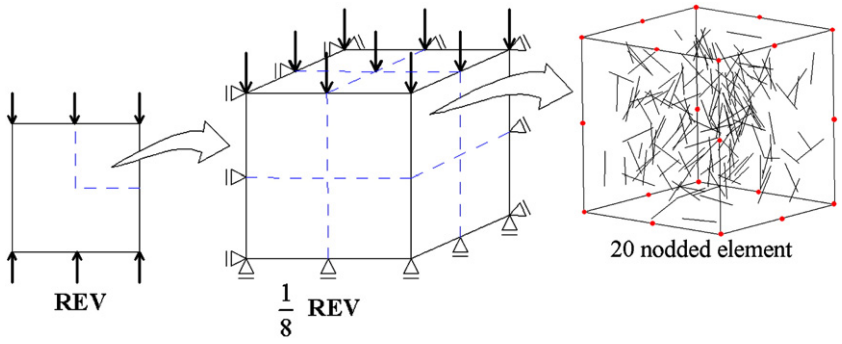

Fig. 10. REV under uniaxial compression considered for the FE simulations.

The homogenized elastic parameters are then obtained by $E^{\hom} = \sum_l / E_l$ and $\nu^{\hom} = E_t / E_l$.

In the objective to qualitatively address the scale effect, two values for the REV side $l = 20, 40$ cm as well as two values for the fiber length $d = 1, 3$ cm have been considered in the numerical study. The values adopted for the aspect ratio and volume fraction of fibers range between 10–100 and 0.5%–5%, respectively.

For each of the above configuration defined by the set $\{l, d, \alpha, f\}$, several random generated distributions of fibers have been considered, and the average values of computed $E^{\hom}$ and $\nu^{\hom}$ were retained as numerical estimates for the homogenized elastic parameters.

The numerical results are given in Tables 3 and 4, where the Mori–Tanaka predictions are also reported. It is noted that $E^{\hom}_{\text{mean}}$ and $\nu^{\hom}_{\text{mean}}$ stand for the mean values of the effective Young modulus and Poisson ratio obtained from the FE simulations, SD and CV are the corresponding standard deviation and coefficient of variation.

As it clearly appears from the above results, the micromechanical predictions are very close to the FE numerical solutions. This emphasizes the consistency of the Mori–Tanaka scheme to estimate the elastic properties of FRC. In addition even though the condition $d \ll l$ necessary for scale separation is roughly satisfied for the adopted values of d and l, the obtained results seem to be low sensitive to the value of ratio d/l, at least for the considered data. This justifies that the volume of FRC tested in the numerical simulation has the status of REV.

Remark

Clearly enough, addition of steel fibers in amounts as small as those commonly used for FRC has a negligible effect on the effective elastic properties. From a practical point of view, computing the effective elasticity of FRC is not in itself a relevant task. However, this is a necessary step for further upscaling towards the formulation of a consistent micromechanical model describing the overall elastoplastic behavior of FRC.

3. Non-ageing viscoelastic behavior of FRC

Under constant load, a concrete specimen first exhibits instantaneous elastic deformation then followed by a slow further increase of deformation in time, corresponding to concrete creep phenomenon. Incorporation of fibers such as steel fibers in concrete reduces the magnitude of creep deformation and associated damage, as has been well experimentally evidenced by Mangat and Azari [41]. The mechanism at the basis of the effect of fiber on matrix creep strain which is frequently invoked relies on the assumption that shear stress is induced at the fiber/matrix interface. Fibers do provide restraint to the sliding action of the matrix relative to the fiber due to the flow component of creep.

However, up to now, few works have been dedicated to linking macroscopic FRC creep behavior to composite micromechanics. Furthermore, the models developed in this context are essentially restricted to uniaxial creep of FRC [41,42].

This section is devoted to the investigation of macroscopic non-ageing viscoelastic properties of FRC. Basically, the approach consists in taking advantage of elastic homogenization in Laplace (or Laplace–Carson) transform framework and making use of the correspondence principle (see for instance [43,44]). Formally, the concentration problem to be solved for non-ageing viscoelastic constitutive materials is identical to the elastic case defined by Eq. (4). The constitutive equations at the macroscopic scale are therefore obtained by inverse Laplace (or Laplace–Carson) transform.

Table 3
FE element calculations and Mori–Tanaka prediction of the homogenized Young modulus of FRC.

Fiber		$d = 3$ cm				$d = 1$ cm				Mori–Tanaka
REV		$l = 20$ cm			$l = 40$ cm	$l = 20$ cm			$l = 40$ cm	
α	f(%)	Young modulus			Young modulus	Young modulus			Young modulus	
		$E^{\hom}_{mean}$ (MPa)	SD	CV	E (MPa)	$E^{\hom}_{mean}$ (MPa)	SD	CV	E (MPa)	E (MPa)
10	0.5					3105.84	0.81	0.00026	3106.56	3129.42
	1					3134.53	1.83	0.00058	3132.55	3159.03
	3	3252.19	13.75	0.0042	3252.29	3248.33	3.16	0.00097		3279.51
	5	3363.14	14.80	0.0044	3363.62	3366.44	2.68	0.00080		3403.31
40	3	3245.41	4.84	0.0015	3245.51					3293.72
	5	3353.86	5.46	0.0016	3353.91					3427.13
80	3	3245.37	1.94	0.0006						3295.24
	5	3354.28	1.98	0.0006						3429.68
100	3	3247.37	1.85	0.0006						3295.46
	5	3353.88	1.94	0.0006						3430.05

Table 4
Homogenized Poisson ration of FRC: FE calculations and Mori–Tanaka predictions.

Fiber		$d=3$ cm				$d=1$ cm				Mori–Tanaka
REV		$l=20$ cm			$l=40$ cm	20 cm			40 cm	
α	f(%)	Poisson ratio			Poisson ratio	Poisson ratio			Poisson ratio	
		ν_{mean}^{hom}	SD	CV	ν	ν_{mean}^{hom}	SD	CV	ν	ν
10	0.5					0.203	0.00009	0.0004	0.204	**0.200**
	1					0.205	0.00011	0.0006	0.205	**0.201**
	3	0.209	0.0012	0.0059	0.209	0.209	0.00013	0.0006		**0.203**
	5	0.214	0.0013	0.0060	0.214	0.214	0.00024	0.0011		**0.205**
40	3	0.209	0.0002	0.0011	0.209					**0.203**
	5	0.213	0.0004	0.0017	0.213					**0.205**
80	3	0.209	0.0002	0.0009						**0.203**
	5	0.213	0.0001	0.0003						**0.205**
100	3	0.209	0.0001	0.0005						**0.203**
	5	0.213	0.0002	0.0010						**0.205**

In non-ageing viscoelasticity, the local stress tensor in the REV is related to the strain history by means of the hereditary Boltzmann integral representation

$$\underline{\underline{\sigma}}(\underline{x},t) = \underline{\underline{\varsigma}}(\underline{x}) \circ \underline{\underline{\varepsilon}}(\underline{x}) = \int_{-\infty}^{+\infty} \underline{\underline{\underline{\underline{\varsigma}}}}(\underline{x},t-\tau) : \dot{\underline{\underline{\varepsilon}}}(\underline{x},\tau) d\tau \tag{12}$$

where $\underline{\underline{\underline{\underline{\varsigma}}}}$ refers to the fourth-order relaxation modulus tensor and $\dot{\underline{\underline{\varepsilon}}} = \partial \underline{\underline{\varepsilon}} / \partial \tau$ is understood in sense of distribution in order to account for possible discontinuities in time. The argument 't' accounts for the instantaneous response of the viscoelastic material while the argument 't' stands for the whole past history of $\underline{\underline{\varepsilon}}$ (the dependence on τ characterizes the delayed response).

The indication of spatial dependence, that is, the dependence on the position vector x will be omitted in the sequel.

Recalling that the Carson–Laplace transform of function $F(t)$ is defined as

$$F^*(p) = p \int_{-\infty}^{+\infty} F(t-\tau) e^{-pt} dt \tag{13}$$

so that the viscoelastic relationship writes in terms of Carson–Laplace transforms

$$\underline{\underline{\sigma}}^* = \underline{\underline{\underline{\underline{\varsigma}}}}^* : \underline{\underline{\varepsilon}}^* \tag{14}$$

which formally expresses an elastic type relationship in Carson–Laplace space. The elastic homogenization procedure carried out in Section 2 as well as related results hold in terms of Carson–Laplace transform fields. The macroscopic stress and strain transforms are related through $\underline{\underline{\Sigma}}^* = \underline{\underline{\underline{\underline{\varsigma}}}}^{hom*} : \underline{\underline{E}}^*$ in which $\underline{\underline{\underline{\underline{\varsigma}}}}^{hom*}$ represents the Carson–Laplace transform of the macroscopic elasticity tensor. In particular, the Carson–Laplace transform of the Mori–Tanaka estimate $\underline{\underline{\underline{\underline{\varsigma}}}}^{hom,MT*}$ can be used as approximation of $\underline{\underline{\underline{\underline{\varsigma}}}}^{hom*}$ (i.e., $\underline{\underline{\underline{\underline{\varsigma}}}}^{hom*} \approx \underline{\underline{\underline{\underline{\varsigma}}}}^{hom,MT*}$).

To go further, we shall first specify the viscoelastic behavior of each constituent of FRC.

3.1. Behavior of concrete matrix and steel fibers

As a first approximation, the uniaxial non-ageing viscoelastic behavior of concrete matrix is described by the Zener rheological model [44,45] shown in Fig. 11. This simple and commonly used model for linear viscoelastic solid consists in the association in series of a spring (stiffness E_1) and a Kelvin element with spring stiffness E_2 and dashpot viscosity η. Even though this model is conceptually very simple, it reasonably describes the main expected characteristics of the response under creep and relaxation observed experimentally for concrete [43,46].

The relaxation compliance $E^{zener}(t)$ associated to the Zener model reads

$$E^{zener}(t) = \frac{E_1}{E_1 + E_2}(E_2 + E_1 e^{-t/\tau_r}) \tag{15}$$

where $\tau_r = \frac{\eta}{E_1 + E_2}$ is the relaxation characteristic time. It is observed that $E^{zener}(0) = E_1$ and $E^{zener}(+\infty) = \frac{E_1 E_2}{E_1 + E_2}$ respectively refer to the instantaneous and asymptotic relaxation moduli.

To describe the three-dimensional non-ageing viscoelastic behavior of isotropic concrete matrix, the relaxation modulus under tensile stress is first approximated by the Zener relaxation compliance (Eq. (15)), while a constant Poisson ratio ν^m is adopted [47–49].

$$E^m(t) = E^{zener}(t) H(t) \; ; \; \nu^m(t) = \nu^m H(t) \tag{16}$$

where $t \to H(t)$ is the Heaviside step function. The stiffness parameters of the model are identified by observing that E_1 represents the elastic instantaneous stiffness, while the asymptotic relaxation modulus $E(+\infty)$ ranges between 3 and 5 times the instantaneous stiffness E_1, depending on certain parameters such as the quality of concrete, humidity and temperature [45,50,51]. As regards the viscosity coefficient η, its value may be evaluated from the value of the characteristic time in relaxation τ_r, which usually ranges between 100 and 300 days [45,51,52].

Finally, the analysis is restricted herein to steel fibers, for which the delayed effects can be neglected at usual temperatures. Accordingly, a linear elastic behavior is adopted for fibers, E^f and ν^f being the Young modulus and Poisson ratio of steel, respectively.

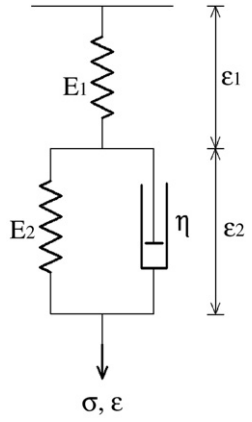

Fig. 11. Zener Model for uniaxial non-ageing viscoelastic behavior of concrete matrix.

3.2. Homogenized viscoelastic properties of FRC

As mentioned in the previous section, we first proceed to elastic homogenization in the space of Carson–Laplace transforms. The initial step is to compute the transforms of the bulk and shear moduli of concrete (k^{m*},g^{m*}), and of steel (k^{f*},g^{f*}).

The correspondence principle indicates that the Carson–Laplace transforms of the homogenized bulk and shear moduli of FRC are formally obtained by replacing in the expressions of $K^{\hom}$ and $G^{\hom}$ the bulk and shear moduli of FRC components by their Carson–Laplace transforms. For simplicity, we shall restrict the subsequent analysis to the situation of fibers with infinite value for the aspect ratio ($\alpha\to+\infty$). Hence, referring to Eqs. (A1) and (A4) of the Appendix, one has

$$K^{\hom*} = \frac{N_K(k^{m*}, g^{m*}, k^{f*}, g^{f*}, f)}{D_K(k^{m*}, g^{m*}, k^{f*}, g^{f*}, f)} \tag{17}$$

$$G^{\hom*} = \frac{N_G(k^{m*}, g^{m*}, k^{f*}, g^{f*}, f)}{D_G(k^{m*}, g^{m*}, k^{f*}, g^{f*}, f)} \tag{18}$$

The crucial step of such a viscoelastic homogenization process lies in the ability to compute the Carson–Laplace inverse transform of Eqs. (17) and (18). Generally, such an inverse transform is achieved by means of numerical procedures such as those given in Abate and Whitt [53].

In the present situation, the particular structure of Eqs. (17) and (18) makes it possible to derive analytically the expression of the relaxation moduli $K^{\hom}(t)$ and $G^{\hom}(t)$. The latter moduli can formally be written as

$$K^{\hom}(t) = \left[Q_0 + \sum_{j=1}^{2} \frac{Q_j}{q_j}(1-e^{-q_j t})\right] H(t) \tag{19}$$

and

$$G^{\hom}(t) = \left[R_0 + \sum_{j=1}^{4} \frac{R_j}{r_j}(1-e^{-r_j t})\right] H(t) \tag{20}$$

where coefficients Q_j, R_j, q_j and r_j are known functions of E_1, E_2, η, v^m, E^f, $v^f$and f.

The above viscoelastic behavior of FRC is illustrated below. The select data corresponding to the usual concrete and steel fibers are given in Table 5. The parameters of the Zener model describing the viscoelastic behavior of concrete are $E_1=31$ GPa, $E_2=15.43$ GPa, $\eta=4650$ GPa×days. The fact that these model parameters are considered as constant is consistent with the approximation of non-ageing concrete behavior. It is observed that the latter could reasonably be justified for instance if concrete is loaded at advanced age [46].

The variations in time of the creep compliance function in bulk $J_K^{\hom}(t)$ and creep compliance in shear $J_G^{\hom}(t)$ are displayed in Fig. 12 and Fig. 13, respectively. It should be recalled that these functions are related to $K^{\hom}(t)$ and $G^{\text{home}}(t)$ in the Carson–Laplace domain through

Table 5
Viscoelastic model data.

Concrete	Instantaneous relaxation modulus	$E^m(0)$	31,000 MPa
	Asymptotic relaxation modulus	$\varepsilon^m(+\infty)$	10,300 MPa
	Relaxation time	τ_r	100 days
	Poisson ratio	v^m	0.2
Steel	Young modulus	E^f	210,000 MPa
	Poisson ratio	v^f	0.3

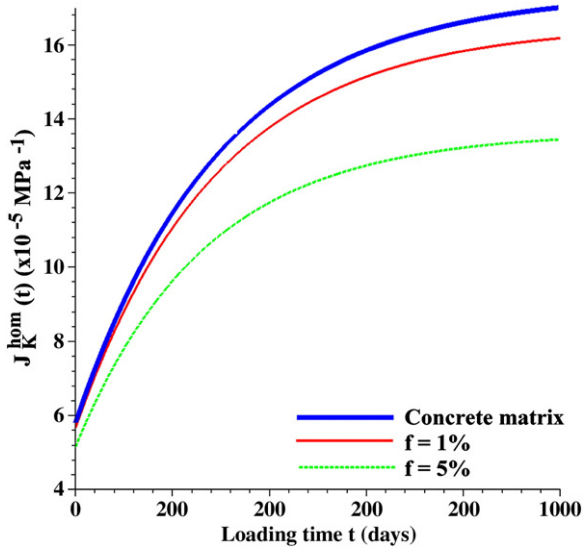

Fig. 12. Model-predicted creep compliance bulk for steel (FRC) for two values of fiber volume fraction.

$J_K^{\hom*}=1/K^{\hom*}$ and $J_G^{\hom*}=1/G^{\hom*}$. Two values commonly used for steel (FRC) have been considered: $f=1\%$ and $f=5\%$.

As shown by Figs. 12 and 13, the addition of steel fibers

- does not significantly affect the elastic instantaneous properties;
- does provide restraint to the deformation of the concrete matrix along the fiber matrix interfacial bond.

These observations are consistent with previous works [41,54]. Besides, these figures clearly show that the reinforcing effect due to fibers increases with time. Finally, it also appears from these figures that the so-called 'memory effects', generally induced by homogenization (see for example [55]), are not significant in the present case as it can be illustrated trough a comparison between the relaxation characteristic times of concrete and homogenized materials. Indeed, the characteristic time for the variations of $G^{\hom}$ is about 102 days whereas it is equal to 100 days for the considered concrete. This small difference is attributed to the particular viscoelastic model considered for concrete as well as to the selected data. It is likely that the memory effects would be more important if the amount of fiber increases.

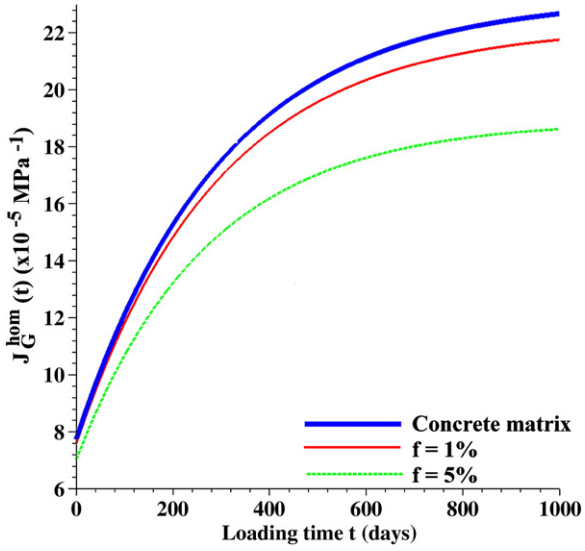

Fig. 13. Model-predicted creep compliance in shear for steel FRC for two values of fiber volume fraction.

4. Validation of the viscoelastic model

This section is intended to validate and verify the proposed theory and model for non-ageing viscoelastic behavior of FRC. The model predictions will be compared to available experimental data as well as to some theoretical models already developed for the compressive creep of concrete matrix reinforced by steel fibers.

It should be kept in mind that only non-ageing basic creep of concrete is addressed in the proposed model. All the other components and mechanisms of concrete creep, as briefly described hereafter, are disregarded in the modeling.

In addition to load-induced creep strains, concrete exhibits time-dependent strains also under free-stress conditions. These strains are referred to as shrinkage strains and arise due to changes in temperature (thermal shrinkage) and/or to changes in the water content. The latter changes result from the hydration process (autogeneous shrinkage deformation) and/or from drying of the material (drying shrinkage deformation).

Moreover, in the context of solidification theory proposed by Bažant and Prasannan [56,57] and corroborated by extensive data fitting and verification, both ageing and non-ageing components of basic creep are not controlled by the hydration degree only, but also by the growth in effective load-bearing volume fraction of hydrated cement. This fraction can continue to grow significantly up to high ages as a result of progressive formation of bonds among the solid particles of hydrated cement.

4.1. Model predictions versus experimental results

An experimental investigation on creep of steel fiber reinforced concrete has been performed by Mangat and Azari [41]. The tests were carried out on specimens 100 mm × 100 mm × 500 mm of concrete reinforced by means of steel fibers with aspect ratio ranging between $\alpha = 56$ and $\alpha = 61$. The volume fraction of fibers ranged between $f = 0$ and $f = 3\%$. The specimens were cured in a temperature and humidity controlled room for 28 days and then loaded under uniaxial compression up to a stress/strength ratio of 0.3. A temperature of 20 °C and a relative humidity of 55% were maintained in the controlled curing room. Table 6 summarizes the properties of the materials used for the experimental analysis.

For comparison purpose, the procedure used to identify the model parameters (Zener parameters) is the following. The instantaneous relaxation modulus is determined by condition $E^{\text{zener}}(0) = E_1 = \sigma_c / \varepsilon^m(0)$, whereas the value of E_2 is fixed by the asymptotic condition $E^{\text{zener}}(+\infty) = \frac{E_1 E_2}{E_1 + E_2} = \sigma_c / \varepsilon^m(+\infty)$. These conditions yield $E_1 = 20.4$ GPa and $E_2 = 7.7$ GPa. The determination of the dashpot viscosity η, or equivalently the characteristic time in relaxation, is achieved by curve fitting from the experimental creep curve of unreinforced concrete. This leads to the value $\eta = 184.1$ GPa × days. Fig. 14 shows the relationship between uniaxial creep strain of steel FRC and time under load at 0.3 stress/strength ratio. The continuous curves represent to model predictions whereas the symbols refer to the experimental points obtained by Mangat and Azari [41].

It is first recalled that all the theoretical model predictions correspond to the asymptotic value $\alpha \to +\infty$ for the fiber aspect ratio. The relevancy of such a model assumption seems to be justified by the experimental measures. Indeed, the experimental results provided in Mangat and Azari [41] suggest that the value of the fiber aspect ratio α has a slight effect on the creep properties of FRC. Actually, this result confirms that that established in elasticity (small influence of α on the overall elastic properties) still hold in viscoelasticity.

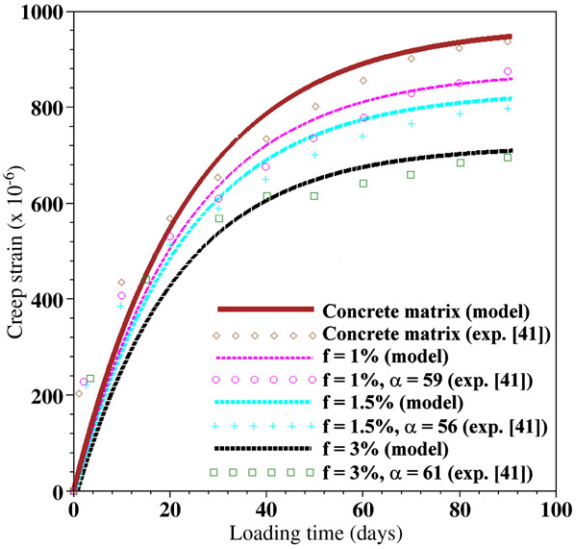

Fig. 14. Creep strain of steel fiber reinforced concrete versus loading time at a stress/strength ratio of 0.3: comparison between model predictions and experiments [41].

It can be seen from this figure that the theoretical predictions fairly fit the experimental results, particularly for advanced loading time. The discrepancy observed at early stages of loading is clearly attributed to the fact that the proposed model does not account for concrete ageing.

The model predictions are now compared to experimental measures performed by Chern and Young [54]. These authors investigated the creep performance of steel fiber reinforced concrete by means of uniaxial compressive tests on 15 cm × 30 cm cylindrical specimens. The FRC specimens have been cured at different values of temperature and relative humidity and then loaded at a stress/strength ratio of 0.25 approximately. The comparison between the model predictions and the experiments will be restricted in sequel to specimens cured for $t' = 28$ days and tested in a room at a temperature of 23 °C and a relative humidity of 50%. The material properties for concrete and steel fibers are summarized in Table 7.

The procedure adopted to identify the model parameters is similar to that used for the comparisons with the results of Mangat and Azari [41]. It leads to $E_1 = 23.5$ GPa, $E_2 = 4.4$ GPa and $\eta = 184.7$ GPa × days. The comparison between model predictions and experimental results in terms of creep function $J(t',t)$ versus loading age curves are shown in Fig. 15. It is recalled that $J(t',t)$ represents the strain at time t caused by a unit sustained load acting since time t'. As previously specified, the value of the latter parameter is $t' = 28$ days.

Unlike the observations made by Mangat and Azari [41], the experimental measures of creep function obtained by Chern and Young [54] are very close for $f = 1\%$ and $f = 2\%$. The above figure suggests that the proposed model predictions underestimate the restraining effect on concrete matrix creep due to the addition of fibers. This question remains however to be confirmed by further comparisons with experimental data.

Table 6
Material properties for creep tests by Mangat and Azari [41].

Concrete	Instantaneous elastic strain	$\varepsilon^m(0)$	$365 \cdot 10^{-6}$
	Asymptotic creep strain	$\varepsilon^m(+\infty)$	$1335 \cdot 10^{-6}$
	Poisson ratio	ν^m	0.2
Steel fiber	Young modulus	E^f	210,000 MPa
	Poisson ratio	ν^f	0.3

Table 7
Concrete and fiber properties for creep tests by Chern and Young [54].

Concrete	Instantaneous elastic strain	$\varepsilon^m(0)$	$290 \cdot 10^{-6}$
	Asymptotic creep strain	$\varepsilon^m(+\infty)$	$1833 \cdot 10^{-6}$
	Poisson ratio	ν^m	0.2
Steel fiber	Young modulus	E^f	210,000 MPa
	Poisson ratio	ν^f	0.3

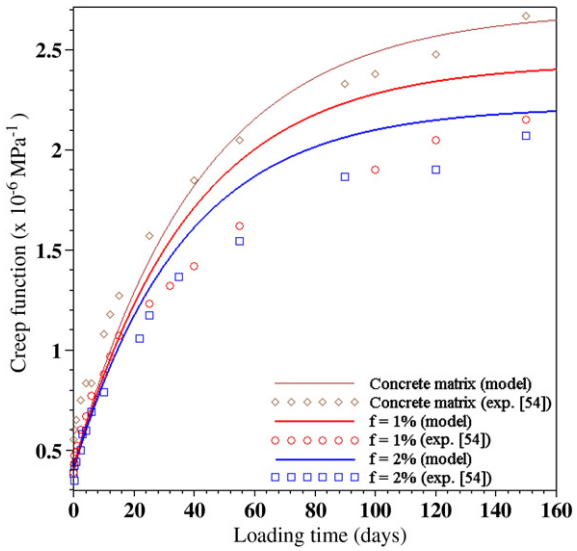

Fig. 15. Creep function versus loading time for steel fiber reinforced concrete loaded at a stress/strength ratio of 0.25: comparison between model predictions and experimental measures [54].

Remark. The model calibration disregards most of the mechanisms described in the beginning of Section 4 and involved in the time-dependent deformation of concrete, such as shrinkage phenomena or dependence of non-ageing properties on effective load-bearing structure of calcium silicate hydrates (C-S-H). Consequently, the results as well as the related comments of comparison of model predictions with experimental data should be considered with caution.

4.2. Model predictions versus existing theoretical results

Additionally to experimental validation, the predictions of the proposed model are compared in the subsequent analysis to those derived from two models available in literature. Mangat and Azari [41] and later Zhang [42] developed analytical models for creep of steel reinforced concrete under uniaxial compression. These two models were formulated within quite similar frameworks in terms of basic assumptions. First, both models are based on the assumption that creep of the reinforced material in the loading direction is restrained by an equivalent distribution of aligned fibers parallel to the direction of sustained applied stress. In addition, the two models assume that the fibers provide restraint to creep of the concrete matrix through the fiber/matrix interfacial shear stress τ. The formulation of the analytical expression for creep strain of steel reinforced concrete matrix is achieved in the approach developed by Mangat and Azari [41] as well in that proposed by Zhang [42] by introducing heuristic considerations.

Figs. 16 and 17 show the predictions of the proposed model together with those derived from the model of Mangat and Azari [41] in terms of creep strain versus loading time for the data given in Table 6. The experimental results obtained by these authors are also reported in these figures for two values of the fiber aspect ratio $\alpha = 56$ and $\alpha = 59$. It is observed from these figures that both models exhibit a good correlation with the experiments, with a rather better agreement between experiments and the proposed model for increasing values of the loading time.

Comparison of the proposed model predictions with those derived from the model of Zhang [42] are shown in Figs. 18 and 19, together with the experimental measures presented in Mangat and Azari [41]. The input data is that given in Table 6. Once again, the two models reasonably agree with the experimental results. The model of Zhang [42] better fit the experiment results for early stages of loading, whereas the proposed model presents better predictions with respect to experiments for higher values of loading time.

Therefore, it can be emphasized from the above analysis that, although its relative simplicity, the proposed viscoelastic model showed:

- A good correlation with a series of experimental results available from two independents studies.
- Similar performance when compared to two analytical models formulated for uniaxial creep of FRC. The main advantage of the proposed model lies in its applicability to multiaxial solicitations.

Clearly enough, the proposed model still needs to be improved in order to address important aspects of FRC behavior, such as ageing or micro-cracking of the matrix. The model can however be used in its current form, as a preliminary approach, in both material optimization and performance prediction with regard to creep of FRC.

5. Conclusion

The macroscopic behaviors in elasticity and non-ageing viscoelasticity of fiber reinforced concrete have been formulated within the framework of homogenization theory for randomly heterogeneous materials.

A Mori–Tanaka linear scheme is first implemented to estimate the effective elastic properties of FRC from the knowledge of the elastic properties of its individual constituents. This model successfully predicts the values of the Young's modulus and Poisson's coefficient of such a composite, as emphasized by comparison with either finite element solutions developed in the present work or available experimental data. A considerable advantage of the micromechanical approach lies in the fact that the closed-form expression for the

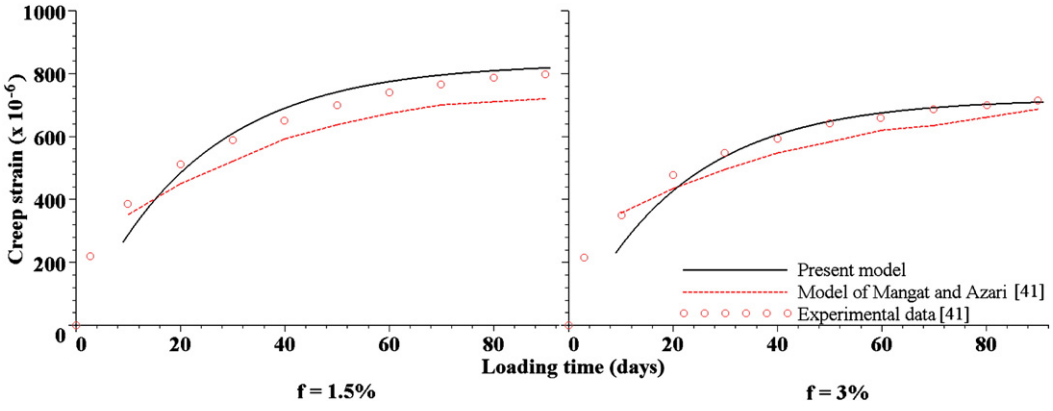

Fig. 16. Creep strain as a function of loading time for fiber aspect ratio$\alpha = 56$. Predictions of proposed model versus predictions of Mangat and Azari [41] model.

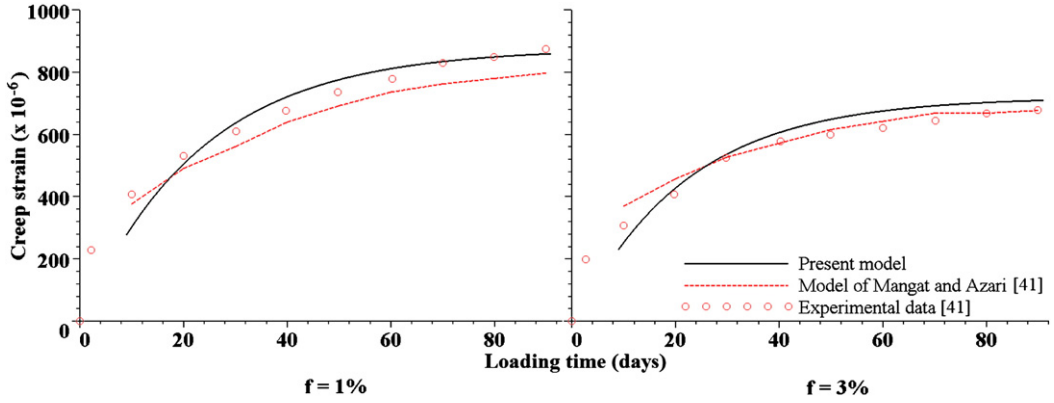

Fig. 17. Creep strain as a function of loading time for fiber aspect ratio $\alpha = 59$. Predictions of proposed model versus predictions of Mangat and Azari [41] model.

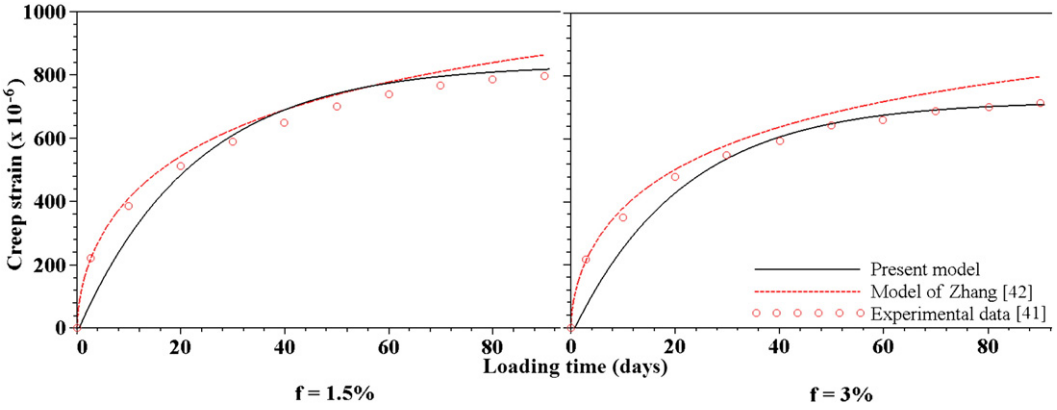

Fig. 18. Creep strain as a function of loading time for fiber aspect ratio $\alpha = 56$. Predictions of proposed model versus predictions of Zhang [42] model.

homogenized elastic properties makes it possible to easily analyze the impact at the macroscopic level of the reinforcement characteristics (fiber stiffness, fiber volume fraction, and fiber aspect ratio).

In the situation, covering in particular the case of loading applied to concrete at advanced age, where ageing could be neglected for the viscoelastic behavior of concrete, the homogenized behavior of FRC has been determined. Reasoning within the framework of Carson–Laplace transform, the conjunction of the results previously obtained in elastic homogenization with the correspondence principle allows deriving closed-form expressions for the homogenized bulk and shear relaxation moduli. The validity of the model has been assessed by mean of comparison with available experiment results of creep strain of FRC specimens under compressive load. It should be emphasized that the experimental results analyzed in this paper clearly indicate no slip on the matrix–fiber interface, which is compatible with the micromechanical model assumptions.

In addition, the model predictions prove to be similar to those derived from two analytical models formulated in one-dimensional setting. The main advantage of the present model lies in its potential applicability to FRC under multiaxial solicitation.

In view of a more comprehensive modeling of FRC behavior, a number of improvements and developments are still necessary. In this

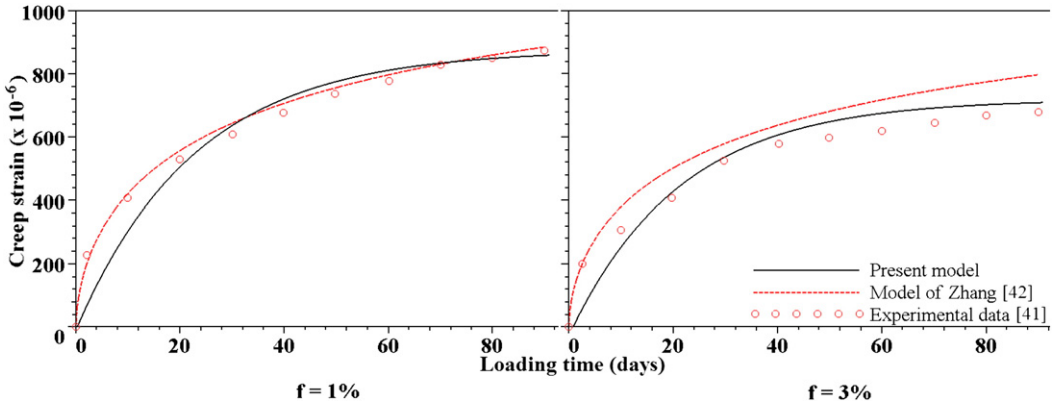

Fig. 19. Creep strain as a function of loading time for fiber aspect ratio $\alpha = 59$. Predictions of proposed model versus predictions of Zhang [42] model.

respect, the validation of the homogenized viscoelastic model formulated in Section 3 through comparison with experimental data and finite element solutions is a fundamental issue to be addressed. As regards the theoretical aspect, a key challenge for next future extensions is to account for ageing. Indeed, the viscoelastic behavior concrete exhibits ageing and a specific homogenization procedure is required [55], since the reasoning based on Carson–Laplace transform does not apply.

Finally, the real task which remains to be done consists in dealing with non-linear phenomena which are necessary for addressing strength. Actually, the formulation of the macroscopic strength properties of FRC by means of limit analysis homogenization techniques is the matter of on-going research.

Appendix A

*Expressions of K^{hom} and G^{hom} for fibers with infinite aspect ratio ($\alpha\to+\infty$)*Below are provided the analytical expressions of the macroscopic bulk modulus $K^{\hom}$and macroscopic shear modulus $G^{\hom}$ of FRC, derived from a Mori–Tanaka homogenization scheme. The aspect ratio of fibers is assumed as infinite, i.e., $\alpha\to+\infty$.

First,

$$K^{\hom} = \frac{N_K(k^m, g^m, k^f, g^f, f)}{D_K(k^m, g^m, k^f, g^f, f)} \tag{A1}$$

where the function N_K and D_K depend on the elastic properties of the components of FRC as well as on the volume fraction of fibers. The numerators in (A1) writes

$$N_K = (3g^m + g^f)[(1-f)k^m + fk^f] + 3k^m k^f \tag{A2}$$

whereas the denominator has the following expression

$$D_K = (3g^m + gf) + 3(fk^m + (1-f)k^f) \tag{A3}$$

The macroscopic shear modulus is expressed by

$$G^{\hom} = \frac{N_G(k^m, g^m, k^f g, ^f f)}{D_G(k^m, g^m, k^f, g^f, f)} \tag{A4}$$

where $N_G = \sum_{i=1}^{6} n_i$ with

$$\begin{cases} n_1 = 9fk^m k^f (g^f)^3\ ,\ n_2 = 3g^m (g^f)^2 (7fg^f (k^m + k^f) + 15k^m k^f (1+f) + 5g^f k^m) \\ n_3 = (g^m)^2 g^f (35(g^f)^2 (35+37f) + 15k^m g^f (5+3f) + 3k^f g^f (35+17f) + 10k^m k^f (9-f)) \\ n_4 = (g^m)^3 ((g^f)^2 (145+39f) + 21k^m g^f (5-f) + 3k^f g^f (40-19f) + 45k^m k^f (1-f)) \\ n_5 = (g^m)^4 (45k^m (1-f) + 15k^f (1-f) + g^f (125-61f))\ ,\ n_6 = 15(g^m)^5 (1-f) \end{cases} \tag{A5}$$

and $D_G = \sum_{i=1}^{5} d_i$ with

$$\begin{cases} d_1 = 3k^m (g^f)^2 (5g^f (1-f) + 3k^f (5-4f)) \\ d_2 = g^m g^f (35(g^f)^2 (1-f) + 3k^m g^f (25-13f) + 21k^f g^f (5-4f) + 90k^m k^f) \\ d_3 = (g^m)^2 ((g^f)^2 (145-73f) + 15k^m g^f (7+f) + 12k^f g^f (10+3f) + 9k^m k^f (5+4f)) \\ d_4 = (g^m)^3 (9k^m (5+4f) + 3k^f (5+16f) + g^f (125+59f))\ ,\ d_5 = (g^m)^4 (15+49f) \end{cases} \tag{A6}$$

References

[1] A. Zaoui, Continuum micromechanics: survey, J. Eng. Mech. 128 (2002) 808–816.
[2] American Concrete Institute. State-of-the-art report on fiber reinforced concrete, in: Manual of concrete Practice, 93, Detroit, Michigan, 1996 (ACI 544.1R-96).
[3] A. Bentur, S. Mindess, Fibre Reinforced Cementitious Composites, Elsevier Science Publishers, New York, 1990.
[4] P. Casanova, P. Rossi, I. Schaller, Can steel fibers replace transverse reinforcement in reinforced concrete beams? ACI Mater. J. 94 (5) (1997) 341–354.
[5] Y. Kwak, M.O. Eberhard, W. Kim, J. Kim, Shear strength of steel fiber-reinforced concrete beams without stirrups, ACI Struct. J. 99 (2002) 530–538.
[6] C. Cucchiara, L. Mendola, M. Papia, Effectiveness of stirrups and steel fibres as shear reinforcement, Cem. Concr. Compos. 26 (7) (2004) 777–786.
[7] S.A. Ashour, F.F. Wafa, M.I. Kamal, Effect of the concrete compressive strength and tensile reinforcement ratio on the flexural behavior of fibrous concrete beams, Engineering Structures 22 (9) (2000) 1145–1158.
[8] J. Thomas, A. Ramaswamy, Mechanical properties of steel fiber-reinforced concrete, J. Mater. Civ. Eng. 19 (2007) 385–392.
[9] C.D. Atiş, O. Karahan, Properties of steel fiber reinforced fly ash concrete, Constr. Build. Mater. 23 (1) (2009) 392–399.
[10] A.V. Hershey, The elasticity of an isotropic aggregate of anisotropic cubic crystals, Journal of Applied Mechanics 21 (3) (1954) 236–240.
[11] E. Kröner, Self-consistent scheme and graded disorder in polycrystal elasticity, J. Phys. F. Met. Phys. 8 (1978) 2261–2267.
[12] S. Nemat-Nasser, M. Hori, Micromechanics: overall properties of heterogeneous materials, Elsevier, North-Holland, 1993.
[13] W.B. Russel, On the effective moduli of composite materials: effect of fiber length and geometry at dilute concentrations, Journal of Applied Mathematics and Physics 24 (1973) 581–600.
[14] R.M. Christensen, K.H. Lo, Solutions for effective shear properties in three phase sphere and cylinder model, J. Mech. Phys. Solids 27 (4) (1979) 315–330.
[15] Y. Huang, K.X. Hu, X. Wei, A. Chandra, A generalized self-consistent mechanics method for composite materials with multiphase inclusions, J. Mech. Phys. Solids 42 (1994) 491–504.
[16] P.M. Suquet, Elements of homogenization for inelastic solid mechanics, in: E. Sanchez-Palencia, A. Zaoui (Eds.), Homogenization Techniques for Composite Media, Lecture notes in physics No. 272, Springer, New York, 1987, pp. 193–278.
[17] T. Mori, K. Tanaka, Average stress in matrix and average elastic energy of materials with misfitting inclusions, Acta Metall. 21 (1973) 571–574.
[18] Y. Benveniste, A new approach to the application of Mori–Tanaka's theory in composite materials, Mech. Mater. 6 (2) (1987) 147–157.
[19] G.J. Weng, The theoretical connection between Mori–Tanaka's theory and the Hashin–Shtrikman–Walpole bounds, Int. J. Eng. Sci. 28 (1990) 1111–1120.
[20] F.-J. Ulm, G. Constantinides, F. Heukamp, Is concrete a poromechanics material ? A multiscale investigation of poroelastic properties, Material and Structures/Concrete Science Engineering 37 (265) (2004) 43–58.
[21] J. Sanahuja, L. Dormieux, G. Chanvillard, Modelling elasticity of hydrating cement paste, Cem. Concr. Res. 37 (10) (2007) 1427–1439.
[22] T.J.R. Hughes, G.R. Feijoo, L. Mazzei, J.-B. Quincy, The variational multiscale method — a paradigm for computational mechanics, Comput. Methods Appl. Mech. Eng. 166 (1998) 3–24.
[23] T.I. Zohdi, J.T. Oden, G.J. Rodin, Hierarchical modelling of heterogeneous bodies, Comput. Methods Appl. Mech. Eng. 138 (1996) 273–298.
[24] J.T. Oden, V. Kumar, N. Moes, Hierarchical modelling of heterogeneous solids, Comput. Methods Appl. Mech. Eng. 172 (1999) 3–25.
[25] T. Hettich, A. Hund, E. Ramm, Modeling of failure in composites by X-FEM and level within a multiscale framework, Comput. Methods Appl. Mech. Eng. 197 (5) (2008) 414–424.
[26] J.D. Eshelby, The determination of the elastic field of an ellipsoidal inclusion, and related problems, Proceedings of the Royal Society of London. Series A 241 (1226) (1957) 376–396.
[27] G. Faivre, Hétérogénéités ellipsoïdales dans un milieu élastique anisotrope, Journal of Physics 32 (4) (1971) 325–331.
[28] N. Laws, The determination of stress and strain concentrations at an ellipsoidal inclusion in an anisotropic material, J. Elast. 7 (1977) 91–97.
[29] T. Mura, Micromechanics of Defects in Solids, Nijhoff, The Hague, The Netherlands, 1987.
[30] A. Suvorov, G. Dvorak, Rate form of the Eshelby and Hill tensors, Int. J. Solids Struct. 39 (2002) 5659–5678.
[31] R. Hill, A self-consistent mechanics of composite materials, J. Mech. Phys. Solids 13 (4) (1965) 213–222.
[32] B. Budiansky, On the elastic moduli of some heterogeneous materials, J. Mech. Phys. Solids 13 (4) (1965) 223–227.
[33] M. Kachanov, A microcrack model of rock inelasticity — Part I: frictional sliding on microcracks, Mech. Mater. 1 (1982) 19–27.
[34] M. Kachanov, A microcrack model of rock inelasticity — Part II: propagation of microcracks, Mech. Mater. 1 (1982) 29–41.
[35] H. Horii, S. Nemat-Nasser, Overall moduli of solids with microcracks: load induced anisotropy, J. Mech. Phys. Solids 31 (2) (1983) 155–171.
[36] V. Deudé, L. Dormieux, D. Kondo, S. Maghous, Micromechanics approach to nonlinear poroelasticity: application to cracked rocks, J. Eng. Mech. ASCE 128 (8) (2002) 848–855.
[37] V. Pensée, D. Kondo, L. Dormieux, A micromechanical analysis of anisotropic damage in brittle materials, J. Eng. Mech. ASCE 128 (2002) 889–897.
[38] G.R. Williamson, The effect of steel fibers on the compressive strength of concrete, International Symposium on Fiber Reinforced Concrete, SP 44–11, Am. Concr. Inst. (1974) 195–207.
[39] R. Hill, The essential structure of constitutive laws for metal composites and polycrystals, J. Mech. Phys. Solids 15 (2) (1967) 79–95.
[40] A.E. Elwi, T.M. Hrudey, Finite element model for curved embedded reinforcement, J. Eng. Mech.Div. 115 (4) (1989) 740–754.
[41] P.S. Mangat, M.M. Azari, A theory for the creep of steel fibre reinforced cement matrices under compression, J. Mater. Sci. 20 (1985) 1119–1133.
[42] J. Zhang, Modeling of the influence of fibers on creep of fiber reinforced cementitious composite, Compos. Sci. Technol. 63 (2003) 1877–1884.

[43] J. Salençon, Viscoélasticité, Presse de l'Ecole Nationales des Ponts et Chaussées, Paris, 1993.
[44] G.J. Creus, Viscoelasticity: Basic Theory and Applications to Concrete Structures, Springer-Verlag, Berlin, 1986.
[45] P.K. Mehta, P.J.M. Monteiro, Concrete: Microstructure, Properties and Materials, McGraw-Hill, New York, 2006.
[46] A. Berthollet, Contribution à la modélisation du béton vis-à-vis du vieillissement et de la durabilité: interaction des déformations de fluage et du comportement non-linéaire du matériau, PhD Thesis, Ecole doctorale de Mécanique, Energétique, Génie civil et Acoustique, Lyon, 2003.
[47] E.A. Kogan, Creep of concrete under multiaxial compression, Power Technol. and Eng. 17 (1983) 448–452.
[48] Z.P. Bažant, Theory of creep and shrinkage in concrete structures: A precis of recent developments, in: S. Nemat-Nasser (Ed.), Mechanics Today, American Academy of Mechanics, vol 2, Pergamon Press, New York, 1975, pp. 1–93.
[49] K.S. Gopalakrishnan, A.M. Neville, A. Ghali, Creep Poisson's ratio of concrete under multiaxial compression, ACI J. 66 (12) (1969) 1008–1019.
[50] A. Ghali, R. Favre, Concrete Structures: Stresses and Deformations, Chapman and Hall, London, 1986.
[51] A.M. Neville, W.H. Dilger, J.J. Brooks, Creep of Plain and Structural Concrete, Construction Press, London, 1983.
[52] Z. P. Bažant, Creep of concrete, in: K.H.J. Buschow et al. (eds.), Encyclopedia of materials: Science and Technology, Elsevier, Amsterdam, Vol. 2C, 2001, 1797–1800.
[53] J. Abate, W. Whitt, A unified framework for numerically inverting Laplace transforms, INFORMS J Comput 18 (4) (2006) 408–421.
[54] J.C. Chern, C.H. Young, Compressive creep and shrinkage of steel fibre reinforced concrete, The International Journal of cement Composites and Lightweight Concrete 11 (4) (1989) 205–214.
[55] S. Maghous, G.J. Creus, Periodic homogenization in thermoviscoelasticity: case of multilayered media with ageing, Int. J. Solids Struct. 40 (2003) 851–870.
[56] Z.P. Bažant, S. Prasannan, Solidification theory for concrete creep: I. Formulation, J. Eng. Mech. 115 (8) (1989) 1691–1703.
[57] Z.P. Bažant, S. Prasannan, Solidification theory for concrete creep: II. Verification and application, J. Eng. Mech. 115 (8) (1989) 1691–1703.